



RESEARCH PAPER

Neurovascular hypoxia after mild traumatic brain injury in juvenile mice correlates with heart–brain dysfunctions in adulthood

Katherine Leyba¹  | Nitchawat Paiyabhroma² | John P. Salvas¹ | Frederick W. Damen¹ | Alicia Janvier³ | Emma Zub³ | Corinne Bernis⁴ | Richard Rouland⁵ | Christophe J. Dubois⁵ | Jerome Badaut⁵ | Sylvain Richard² | Nicola Marchi³ | Craig J. Goergen¹ | Pierre Sicard² 

¹Weldon School of Biomedical Engineering, Purdue University, West Lafayette, Indiana, USA

²PhyMedExp, INSERM/CNRS/ Université de Montpellier, IPAM/ Biocampus, Montpellier, France

³Institute de Genomique Fonctionnelle, Université de Montpellier, CNRS, INSERM, Montpellier, France

⁴Institut des Maladies Métaboliques et Cardiovasculaires (I2MC), Inserm/ Université Paul Sabatier UMR1048, Toulouse, France

⁵Univ. Bordeaux, CNRS, CRMSB, UMR 5536, Bordeaux, France

Correspondence

Pierre Sicard, INSERM, CNRS, Université de Montpellier, PHYMEDEXP, IPAM/Biocampus, CHU Arnaud De Villeneuve Bât Crastes de Paulet, 371 Avenue du Doyen Gaston Giraud, 34295 Montpellier cedex, France.

Email: pierre.sicard@inserm.fr

Craig J. Goergen, Weldon School of Biomedical Engineering, Purdue University, West Lafayette, IN, USA. Email: cgoergen@purdue.edu

Nicola Marchi, Cerebrovascular and Glia Research, Institut de Génomique

Abstract

Aim: Retrospective studies suggest that mild traumatic brain injury (mTBI) in pediatric patients may lead to an increased risk of cardiac events. However, the exact functional and temporal dynamics and the associations between heart and brain pathophysiological trajectories are not understood.

Methods: A single impact to the left somatosensory cortical area of the intact skull was performed on juvenile mice (17 days postnatal). Cerebral 3D photoacoustic imaging was used to measure the oxygen saturation (sO₂) in the impacted area 4 h after mTBI followed by 2D and 4D echocardiography at days 7, 30, 90, and 190 post-impact. At 8 months, we performed a dobutamine stress test to evaluate cardiac function. Lastly, behavioral analyses were conducted 1 year after initial injury.

Results: We report a rapid and transient decrease in cerebrovascular sO₂ and increased hemoglobin in the impacted left brain cortex. Cardiac analyses showed long-term diastolic dysfunction and a diminished systolic strain response under stress in the mTBI group. At the molecular level, cardiac T-p38MAPK and troponin I expression was pathologic modified post-mTBI. We found linear correlations between brain sO₂ measured immediately post-mTBI and long-term cardiac strain after 8 months. We report that initial cerebrovascular hypoxia and chronic cardiac dysfunction correlated with long-term behavioral changes hinting at anxiety-like and memory maladaptation.

Conclusion: Experimental juvenile mTBI induces time-dependent cardiac dysfunction that corresponds to the initial neurovascular sO₂ dip and is associated with long-term behavioral modifications. These imaging biomarkers of the heart–brain axis could be applied to improve clinical pediatric mTBI management.

Katherine Leyba, Nitchawat Paiyabhroma, and John P. Salvas contributed equally to this work.

Craig J. Goergen and Pierre Sicard jointly supervised this work.

This is an open access article under the terms of the [Creative Commons Attribution-NonCommercial-NoDerivs](https://creativecommons.org/licenses/by-nc-nd/4.0/) License, which permits use and distribution in any medium, provided the original work is properly cited, the use is non-commercial and no modifications or adaptations are made.

© 2023 The Authors. *Acta Physiologica* published by John Wiley & Sons Ltd on behalf of Scandinavian Physiological Society.

Fonctionnelle (University of Montpellier, CNRS, INSERM), 141 rue de la Cardonille, 34094 Montpellier, Cedex 5, France.
Email: nicola.marchi@igf.cnrs.fr

KEYWORDS

4D ultrasound, diastolic dysfunction, heart–brain axis, photoacoustic imaging, traumatic brain injury

1 | INTRODUCTION

Traumatic brain injury (TBI) represents a significant clinical burden.^{1,2} Beyond local brain injury and neuroinflammatory activations,³ TBI could associate with peripheral organ adaptations, with proposed implications of systemic inflammation and autonomic dysregulation.⁴ The effects of TBI on the cardiovascular system are emerging in clinical studies employing echocardiographic examination;⁵ TBI has been associated with a higher risk of chronic cardiovascular comorbidities in adult patients.⁶ These clinical studies focused on moderate–severe TBI in the adult-to-elderly population; however, approximately 80% of all TBI-related emergency room visits are due to mild cases, with unstructured data on the potential pathological trajectories for children under 18 years of age.⁷ Mild TBI (mTBI), or concussion as it occurs in contact sports,⁸ is commonly defined as traumatic biomechanical forces to the brain that do not necessarily lead to a loss of consciousness and shows little to no evidence of structural damage in the CT scan.⁹ The existing knowledge gap calls for preclinical studies to systematically study the functional pathophysiological trajectories of juvenile mTBI at the brain and cardiac levels and pinpoint their temporal associations during adulthood.¹⁰

To address this issue, we examined the long-term cardiac adaptations occurring after experimental juvenile mTBI, retrospectively correlating to brain hypo-oxygenation measures, occurring immediately after mTBI in a mouse-specific manner.¹¹ We used photoacoustic imaging (PAI), which combines laser pulses and high-resolution ultrasound (US) to create multicontrast images of cardiac and brain structures.¹² This noninvasive approach allows an unprecedented monitoring capability of essential heart–brain functions in the same animals and can be repeated over long periods. Although imaging modalities such as magnetic resonance imaging (MRI) can assess left ventricular function, the acquisition is often time-consuming and costly.¹³ The emergence of novel technologies based on United States allows for in vivo assessment of neurovascular and cardiac changes with high specificity.^{11,14,15} Furthermore, we employed high-frequency four-dimensional ultrasound (4DUS), a technique comparable to cine MRI, offering high spatio-temporal resolution to assess cardiac disease progression over time.¹⁶ Our results suggest a post-mTBI correlation between the initial dip in cerebrovascular oxygenation

and long-term cardiac diastolic dysfunction, with adverse long-term adaptations demonstrated in pharmacological cardiac stress tests. Our data also suggest specific long-term behavioral changes post-mTBI that correlate with PAI measures. Collectively, these data unveil coordinated heart–brain maladaptive responses post-juvenile m-TBI that unfolds and persists during adulthood.

2 | RESULTS

2.1 | mTBI triggers immediate regional cerebrovascular hypoxia and increases hemoglobin brain content

We used photoacoustic imaging, repeated over time, to stratify and track the average blood oxygen saturation (mean sO_2 levels) and tissue sO_2 levels (total sO_2) after mTBI in a mouse-specific manner from childhood to adulthood (Figure 1). We recently published a pilot study demonstrating technical feasibility.¹¹ Representative oxygenation maps are shown in Figure 2A. mTBI resulted in a rapid decrease of cerebrovascular sO_2 in the impacted left hemisphere (sham 65.3 ± 6.2 , mTBI 57.21 ± 9.52 , $p = 0.012$; Figure 2B; image example Figure 2A), returning to pre-TBI levels at 7 days and stabilizing long term. Left hemisphere tissue sO_2 levels showed no significant differences between groups. (Figure 2C). Mean HbT was significantly elevated 4 h post-mTBI (sham 2.01 ± 0.45 , mTBI 2.61 ± 0.59 ($\times 10^4$), $p = 0.001$; Figure 2D). HbT returned to pre-TBI levels on day 7. ROC analysis of left hemisphere HbT showed statistical significance (AUC = 0.777, $p = 0.028$) in the ability to distinguish between sham and mTBI 4 h post-mTBI (Figure 2E). However, left hemisphere blood sO_2 (AUC = 0.744, $p = 0.053$) and tissue sO_2 (AUC = 0.570, $p = 0.577$) did not illustrate statistically significant results. In the contralateral hemispheres, sO_2 and HbT measurements showed no significant differences (Figure S1). Corroborating an immediate pathological modification, post-mTBI animals' time to stand was significantly longer compared to the sham group (sham 112.3 ± 107.0 , mTBI 311.6 ± 195.1 , $p = 0.005$). Time to explore the environment was significantly increased in the mTBI group (sham 41.0 ± 43.0 , mTBI 229.8 ± 110.1 , $p = <0.001$), which correlates with the left hemisphere blood hypo-oxygenation levels ($r = -0.541$, $p = 0.006$; Figure S2). In summary, experimental mTBI delivered on

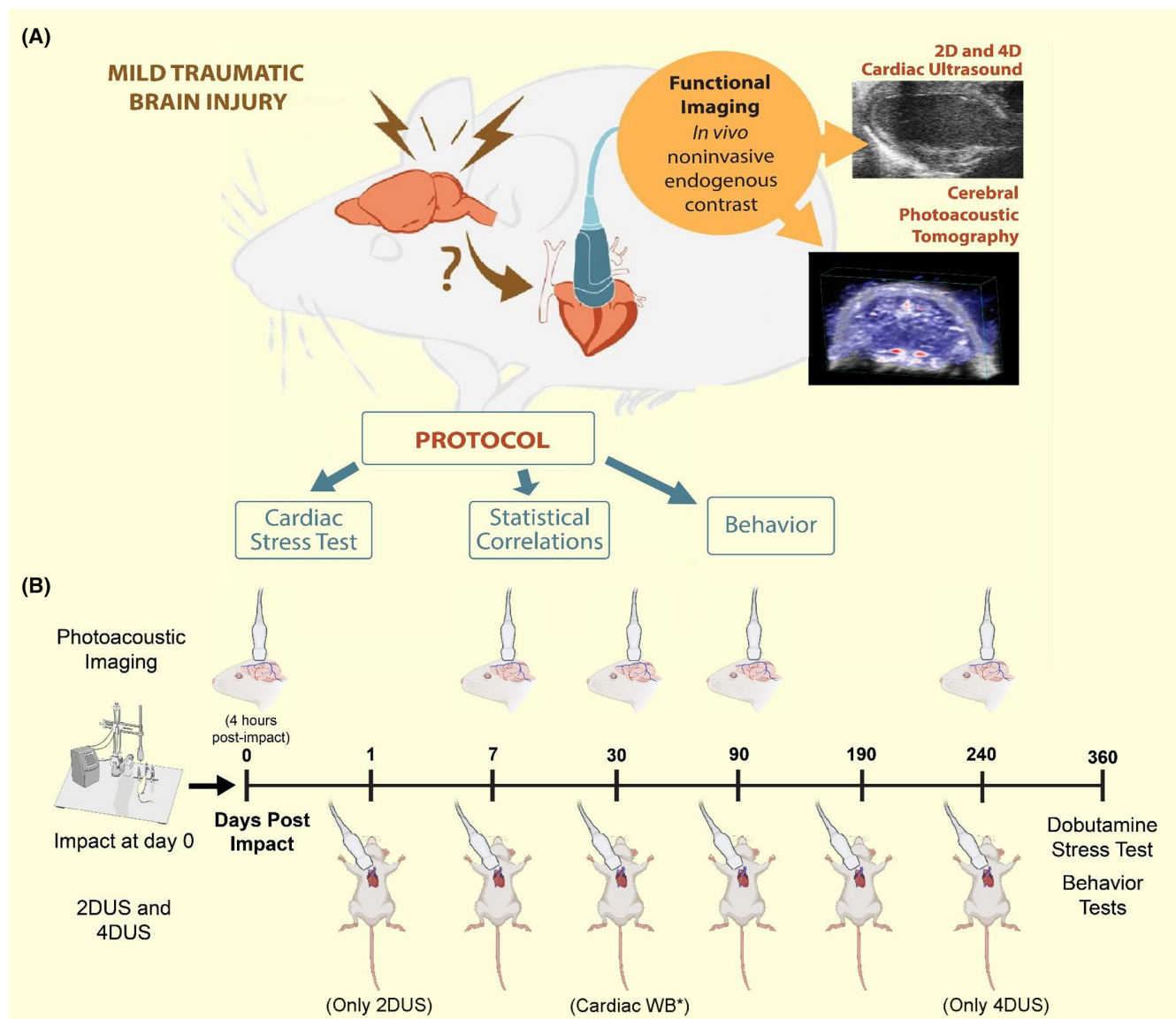


FIGURE 1 Long-term effect of a single mild TBI in juvenile mice on cardiac function and behavior. (A) Experimental design, (B) study timeline. Each dash indicates a time point where we conducted a procedure. Photoacoustic imaging and ultrasound imaging timelines can be visualized with the images above and below the timeline, respectively. Dobutamine stress tests and behavior tests were conducted 360 days post-injury. *Molecular-level pathological signature in the heart was explored by Western blot to assess T-p38 MAPK and cTnI expression on a second batch of animals (sham and mTBI) 1-month post-TBI.

the juvenile brain is sufficient to provoke a transient hypoxic condition with quantitative mouse-specific profiles.

2.2 | mTBI associates with trajectories of sustained diastolic dysfunction with a preserved ejection fraction

A risk for long-term cardiac adaptations in TBI subjects is clinically suspected.⁶ Here, we tested the hypothesis that a mild TBI in juvenile mice is sufficient to elicit adverse cardiovascular trajectories, focusing on cardiac systolic and diastolic function assessed with

4DUS repeated over time (Figure 3A–G). Global LV function metrics such as peak-systolic volume (PSV) and end-diastolic volume (EDV) showed no significant differences between sham and mTBI groups between 7 and 190 days post-injury (Figure 3H,I). While ejection fraction (EF) showed no significant difference between groups from day 7 to 90 post-injury, EF was significantly elevated in the mTBI group at day 190 (sham 56.97 ± 8.82 , mTBI = 63.69 ± 3.65 , $p = 0.034$; Figure 3J). Additionally, while both groups showed a gradual increase in left ventricular mass (LVM) from day 7 to 190 post-injury, LVM was significantly lower in the mTBI group at both day 90 (sham 114.44 ± 16.19 , mTBI 97.68 ± 13.02 , $p = 0.015$)

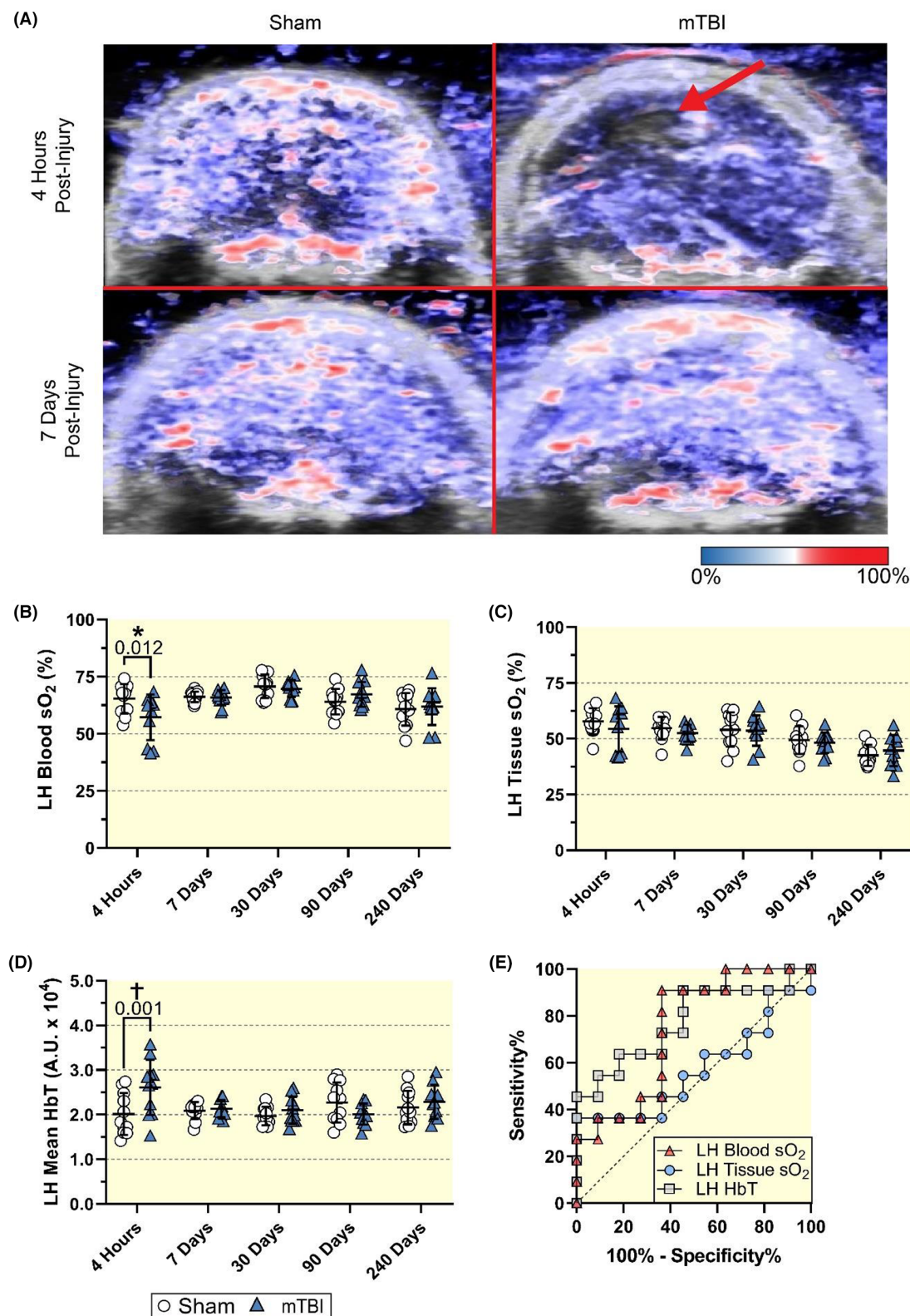


FIGURE 2 Cerebral sO₂ and HbT content altered in the left hemisphere post-traumatic brain injury. (A) Representative photoacoustic images of murine brain 4 h and 7 days post-impact. Color scaling used to show regions of high sO₂ in red and regions of low sO₂ in blue/black in sham and mTBI mice. The arrow indicates the region of impact and lower sO₂. (B) Left hemisphere vascular sO₂ over time. (C) Left hemisphere tissular sO₂ over time. (D) Left hemisphere mean HbT over time. (E) Receiver operating characteristic (ROC) curves of left hemisphere blood sO₂ (AUC = 0.744, $p = 0.053$), tissue sO₂ (AUC = 0.570, $p = 0.577$), and mean HbT (AUC = 0.777, $p = 0.028$) in sham and mTBI mice. Sample sizes are sham $n = 11$ and mTBI $n = 11$. All results are expressed as mean \pm SD.

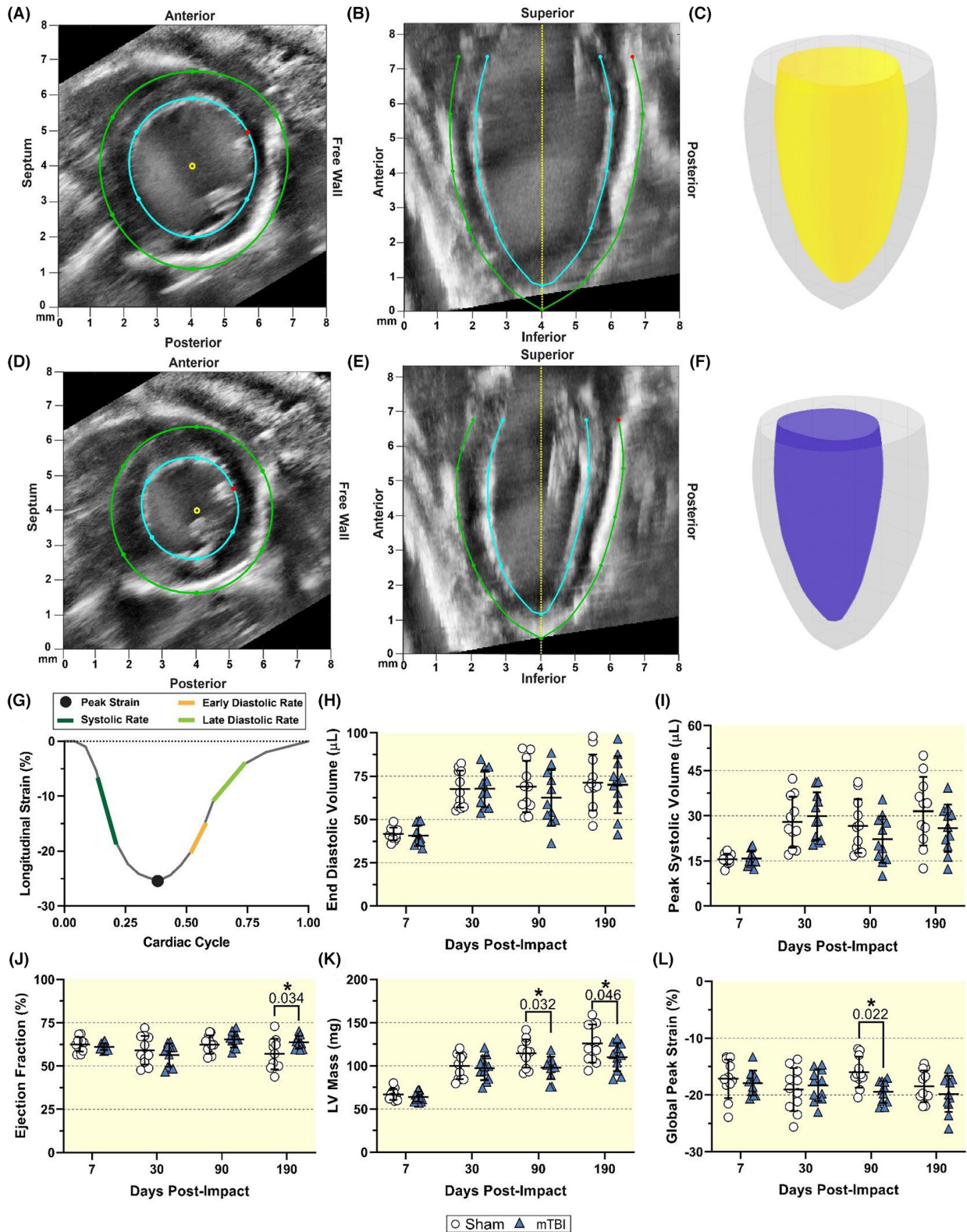


FIGURE 3 Global cardiac function shows little differences in the short and long term. (A) Short and (B) long axes and the (C) 3D volume of the heart at peak diastole extracted from the 4DUS custom toolbox. (D) Short and (E) long axes and the (F) 3D volume of the heart at peak systole extracted from the 4DUS custom toolbox. The manually defined endocardial (blue) and epicardial (green) borders are visualized. (G) Longitudinal strain % map over one cardiac cycle, (H) end diastolic volume, (I) peak systolic volume, (J) ejection fraction, (K) left ventricular mass, and (L) global longitudinal peak strain extracted from the custom toolbox. Sample sizes are sham $n = 11$ and mTBI $n = 11$. Results are expressed as mean \pm SD.

and 190 (Sham 125.84 ± 22.05 , mTBI 109.90 ± 16.21 , $p = 0.046$; [Figure 3K](#)).

We tracked global and regional longitudinal strain using a 4DUS custom analysis to detect ventricular deformation patterns and functional abnormalities. On day 90, a significantly larger global peak strain was observed in the mTBI group (sham -15.94 ± 2.59 , mTBI -19.47 ± 1.84 , $p = 0.022$; [Figure 3L](#)). Global systolic and late diastolic strain rates were not significantly different at any timepoint ([Figure S3](#)). Regional strain analysis showed differences between groups' peak strain in nearly all regions 90 days post-injury. The posterior and posterior-free wall diastolic strain rates, in particular, significantly differed between groups at 90 days post-injury ([Table S1](#)).

Diastolic function was assessed using a combination of several metrics, including left atrial (LA) volume (i.e., capacity for ventricular filling), early diastolic strain rate (i.e., passive ventricular relaxation), and Doppler velocities (i.e., blood flow through the mitral valve) ([Figure 4A–C](#)). LA volume could not be assessed on day 1 due to image quality. At 30, 90, and 190 days post-impact, LA volume in the mTBI group was significantly larger than sham (day 30 $p = 0.034$, day 90 $p = 0.033$, day 190 $p = 0.027$; [Figure 4D](#)). The early diastolic strain rate was decreased in the mTBI group at day 30 (sham 9.17 ± 2.58 , mTBI 6.36 ± 2.06 , $p = 0.006$) and day 190 (sham $9.94 \pm$, mTBI 7.59 ± 1.12 , $p = 0.031$; [Figure 4E](#)). The mTBI group isovolumic relaxation time (IVRT) was lower at day 1 ($p = 0.071$) but was significantly elevated at days 30 (sham 11.60 ± 1.33 , mTBI 13.20 ± 0.99 , $p = 0.009$) and 190 (sham 11.52 ± 1.11 , mTBI 12.84 ± 1.39 , $p = 0.026$; [Figure 4F](#)). To explore early cardiac molecular changes, we performed a Western blot analysis on tissue from sham ($n = 6$) and mTBI animals ($n = 6$) 1 month post-mTBI. We assessed Total p38 mitogen-activated protein kinases (T-p38 MAPK) and cardiac Troponin I (TnI) expression ([Figure 4G](#)). Complete Western blot analyses are provided in supplemental [Figure S4A–C](#). Our results show that mTBI mice exhibit an increase in T-p38 MAPK cardiac expression ($p = 0.039$) and a decrease in cardiac TnI (sham = 1.74 ± 0.32 , mTBI = 1.12 ± 0.28 , $p = 0.005$; [Figure 4H,I](#)). Collectively, these data show that mTBI in juvenile mice induces a diastolic dysfunction with a molecular signature persisting into adulthood.

2.3 | Dobutamine stress test reveals global and regional cardiac dysfunction following mTBI

From these functional 4DUS/Doppler descriptions, we next examined the response of a TBI-heart to stress conditions. To this end, we used an intraperitoneal injection

of the adrenergic agonist dobutamine,¹⁷ a modality that allows revealing long-term dysfunction and perfusion abnormalities. The difference between baseline and post-dobutamine injection peak strain significantly differed in the sham group ($p = 0.000$), while the mTBI displayed no difference in peak strain. The same trend was found in the systolic strain rate where the sham group showed significant differences from pre- to post-dobutamine ($p = 0.000$), and the mTBI group did not ([Figure 5A,B](#)). The changes in early and late diastolic strain rates were lower in the mTBI group but not significant ([Figure 5C,D](#)). Regional strain analysis highlighted significant differences between sham and mTBI early diastolic strain rates in the posterior and posterior-free wall regions of the heart ([Table S2](#)).

The 4DUS strain maps illustrate longitudinal strain pre- and post-injection and the differences between time points and groups ([Figure 5E,F](#)). Individual strain maps are provided in [Figure S5](#). Finally, we used photoacoustic imaging to assess cardiac perfusion overtime during the dobutamine stress test ([Figure 5G–J](#)). The sham group pre- and post-diastolic sO_2 differed ($p = 0.011$), while no statistical significance existed post-mTBI ([Figure 5K,L](#)).

2.4 | Early post-mTBI neurovascular oxygenation correlates with long-term cardiac dysfunction

Thus far, our results show cerebrovascular and cardiac response maladaptations post-mTBI, occurring in a time-dependent and mouse-specific manner. Here, we asked whether direct correlations exist between the examined pathophysiological measures to define prognostic criteria. To this end, we correlated the dataset: Oxygen saturation 4 h post-mTBI and long-term (240 days) peak strain, systolic, early diastolic, and late diastolic strain rate from the dobutamine stress test ([Figure 6A–D](#)). Left hemisphere tissue sO_2 correlated with changes in peak strain ($r = -0.548$, $p = 0.028$) and with late diastolic strain rate ($r = 0.550$, $p = 0.027$) ([Figure 6A,D](#)). Left hemisphere tissue sO_2 was correlated with the changes in systolic ($p = 0.105$) and early diastolic strain rates ($p = 0.056$) ([Figure 6B,C](#)). Left hemisphere hemoglobin content and contralateral sO_2 showed no correlation ([Table S3](#)).

We tested the hypothesis that long-term cardiac dysfunction observed with dobutamine changes could serve as imaging biomarkers to discriminate between sham and mTBI groups. Change in peak strain displayed a statistically significant ROC curve (AUC = 0.810, $p = 0.039$), indicating its ability to discriminate between sham from mTBI animals. Further ROC analyses of other cardiac metrics including changes in systolic strain rate (AUC = 0.730), early diastolic strain rate (AUC = 0.762),

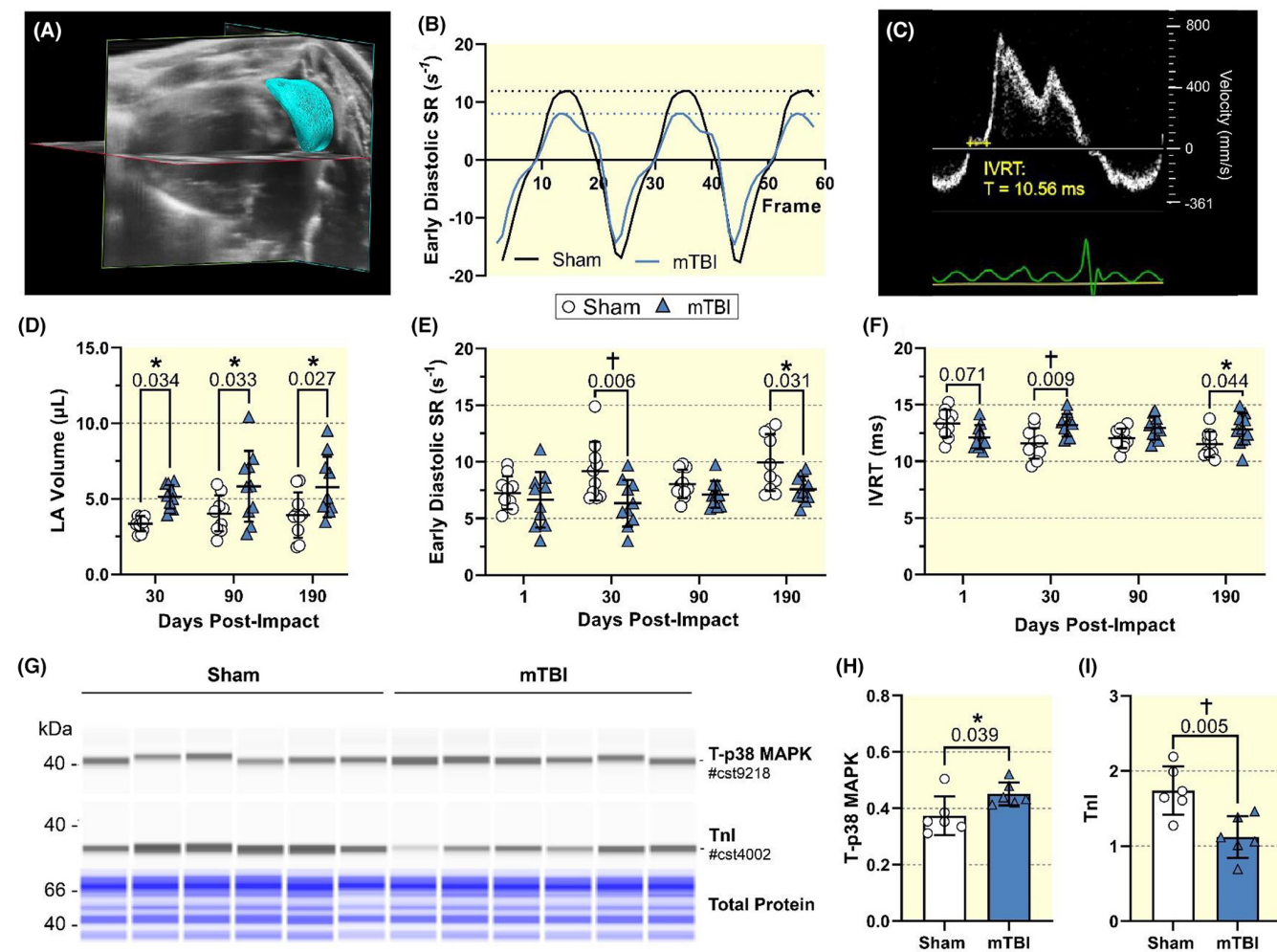


FIGURE 4 Short- and long-term diastolic cardiac function altered after mild traumatic brain injury (A) Representative 4DUS image of the murine heart with a 3D segmentation of the left atrium (LA). (B) Representative early diastolic strain rate curve for sham and mTBI. The three peaks indicate the peak early diastolic strain rate over three cardiac cycles, where the dotted line shows the average value reported. (C) Mitral valve Doppler flow velocity tracing with the isovolumic relaxation time (IVRT) tracing is shown in yellow. The corresponding EKG is below. (D) LA volume. (E) Early diastolic strain rate. (F) Isovolumic relaxation time. All sample sizes sham $n = 10$ and mTBI $n = 10$. (G) Western blot images of cardiac T-p38 MAPK, cardiac TnI, and total protein expression in sham and mTBI 1 month after the insult. (H) Relative level of T-p38 MAPK (AU). (I) Relative level of cardiac TnI (AU). Results are expressed as mean \pm SD. Sample sizes sham $n = 6$ and mTBI $n = 6$.

and late diastolic strain rate (AUC 0.746) could be clinically relevant; however, they showed no statistical significance (Figure S6A–C).

Using principal component analysis (PCA) to highlight the variables showing the most inherent variability in the data, the first two principal components (PCs) explain 62.33% of the variance in the data (Figure 6F). The sham animals are contained to the bottom left quadrant, while the remaining mTBI points are scattered throughout the remaining quadrants. Furthermore, LH mean HbT contributed 9.61% to the weight of the first two PCs. In addition, the inclusion of the changes in global peak strain, end diastolic volume, and diastolic cardiac oxygen saturation increased the cumulative contribution to 38.07% of the weighting (Figure S6D).

2.5 | Heart–brain pathophysiological modifications correlate over time

Subsequently, 1 year after the initial trauma, animals previously tracked using PAI underwent behavioral testing to explore the long-term neurological impact of juvenile mTBI and to unveil possible mouse-specific correlations between heart–brain physiological modifications and behavioral output. Animals were evaluated based on an anxiety-like state (time in the center), locomotor coordination and activity (distance traveled), and memory recognition (discrimination index) (Figure 7A–C). The time in the center was unchanged between groups ($p = 0.162$), suggesting similar basal anxiety levels. However, the mTBI group exhibited a 30% lower distance traveled in the open

field (sham 32.10 ± 8.35 , mTBI 22.10 ± 8.41 , $p = 0.033$) and a significant decrease in discrimination capacity when identifying novel versus familiar objects (familiar 0.93 ± 0.31 , novel 0.38 ± 0.06 , $p = 0.001$; Figure 7D–F). Interestingly, we found that the cerebrovascular blood sO_2 levels, measured 4 h post-mTBI, inversely correlated

with the time in the center ($r = -0.754$, $p = 0.001$) and positively correlated with the distance traveled ($r = 0.513$, $p = 0.042$; Figure 7G,H). Moreover, time in the center positively correlated with hemoglobin content 4 h post-injury ($p = 0.005$; Figure 7I). This result suggests that the severity of brain hypoxia and local hemorrhage 4 h after impact

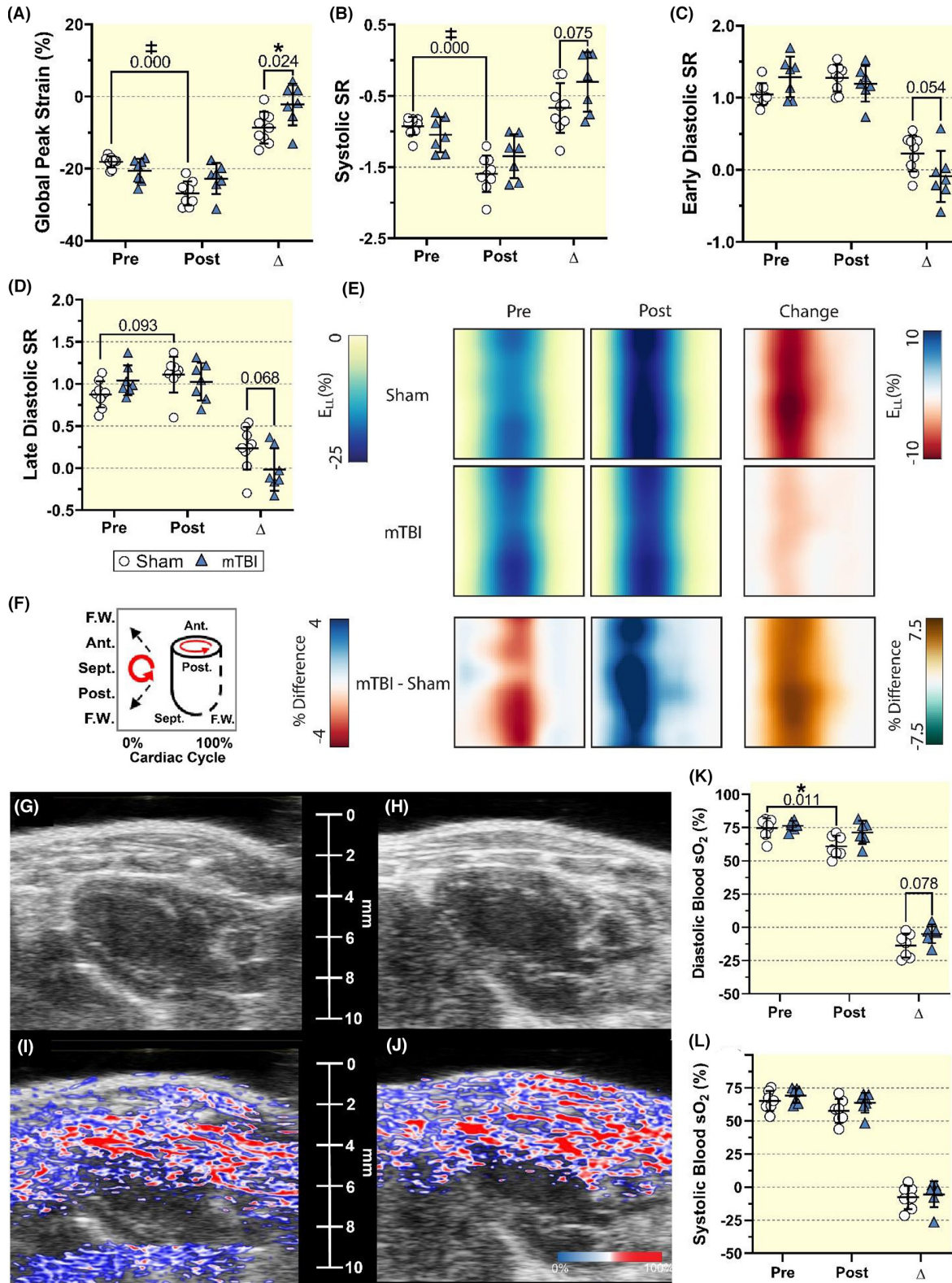


FIGURE 5 Traumatic brain injury affects cardiac strain in dobutamine stress test 8 months after the initial injury. (A) Global longitudinal peak strain, (B) systolic strain rate, (C) early diastolic strain rate, and (D) late diastolic strain rate pre- and post-injection of dobutamine and change between the two. All change metrics were obtained by subtracting post-injection strain from pre-injection strain. Subpanels B–D represent metrics extracted from a custom toolbox with strain rates normalized to one cardiac cycle, thus unitless. (E) Cardiac strain mapping of longitudinal strain over the course of a representative cardiac cycle. The first row of maps depicts sham strain maps pre- and post-injection and blue/red heat map of the change in strain between pre- and post-injection. The second row illustrates similar plots for the mTBI group. The third row depicts the differences between the two maps directly above. Differences were obtained by subtracting mTBI from sham strains. (F) Strain map interpretation key. The vertical axis highlights how regions of the heart are unwrapped on a vertical axis. The horizontal axis represents time in a single cardiac cycle. (G) Sham and (H) mTBI group cardiac ultrasound images. (I) Sham and (J) mTBI cardiac photoacoustic overlaid on the ultrasound image. Photoacoustic color scaling used to show regions of high sO_2 in red and regions of low sO_2 in blue/black. All ultrasound and photoacoustic images are representative images that reflect general trends. (K) Diastolic and (L) systolic myocardial oxygen saturation pre- and post-injection, and the change between the two. All sample sizes are sham $n = 9$, mTBI $n = 7$. Results are expressed as mean \pm SD. We used a two-way ANOVA with Bonferroni post hoc multiple comparisons test for pre- and post-dobutamine comparisons. A studentized t-test was used to compare the change sham versus MTBI.

during juvenile stages may predict the behavioral adaptations during adulthood. Finally, peak strain during the dobutamine test was inversely correlated with novel object discrimination capacity ($p = 0.043$; Figure 7J). These results reveal a predictive value for measuring brain oxygenation early post-mTBI to stratify the risk for long-term, age-dependent adaptations.

3 | DISCUSSION

We demonstrate age-dependent, mouse-specific trajectories of cardiac maladaptations after experimental juvenile mTBI. We found significant correlations between neurovascular hypo-oxygen profiles measured immediately post-mTBI and adulthood heart–brain maladaptation.⁶ Our data resonate with clinical studies suggesting a brain–heart interrelation in TBI subjects. Chronic cardiovascular, endocrine, and neurological outcomes have been reported following brain injuries in patients and rodent models.^{6,18} Our results demonstrate the involvement of the heart–brain axis in mTBI and indicate utility in cardiac monitoring as a possible noninvasive biomarker of disease progression.

3.1 | mTBI and cardiac dysfunction: from juvenile stages to adulthood

Symptoms of cardiac dysfunction have been reported in the short term in adult patients with mild to severe TBI, by evaluating clinical features such as arterial pressure, ejection fraction, and morphological changes in electrocardiograms.^{6,19} Experimentally combining noninvasive 2DUS and 4DUS, we reveal subclinical cardiac dysfunction lingering into adulthood following juvenile mTBI. No changes in cardiac LV morphometry or global function (ejection fraction) were identified in the mTBI group at

rest; however, systolic function decreases in moderate to severe TBI in clinical studies.¹⁰ Interestingly, we found that the mTBI group exhibited changes in LA volume, IVRT, and early diastolic strain rate up to 190 days post-injury, all of which indicate diastolic dysfunction.²⁰ These results align with Cuisinier et al. showing no changes in systolic function but highlighting subclinical diastolic dysfunction with a significant elongation of IVRT in patients with TBI.²¹ Furthermore, molecular analysis of cardiac tissue of the mTBI group found an increase in p38 expression and loss of cardiac TnI (Figure 4H,I). Proteolysis of TnI in the heart is one of the important mechanisms associated with diastolic dysfunction through impaired calcium-dependent muscle contraction.²² Overexpression of p38 MAPK may induce diastolic dysfunction with preserved ejection fraction.²³ Thus, molecular changes of cardiac TnI and T-p38 MAPK further confirm cardiac functional adaptations after mTBI and provide a potential mechanism of action. Furthermore, prospective cohort studies by Krishnamoorthy et al. showed that cardiac dysfunction is present in the short term after TBI and may even revert to baseline within a week.²⁴ However, our study indicates that those effects persist long term.

Dobutamine stress tests, which increase O_2 demand and consumption,²⁵ have revealed underlying cardiac dysfunction in cases of heart failure with preserved ejection fraction.²⁶ Similarly, our model of mTBI-induced diastolic dysfunction with preserved EF showed that a limited stress response correlates with initial oxygen desaturation after injury. Furthermore, the lack of a significant decrease in cardiac sO_2 in the mTBI group suggests impaired myocardial oxygen availability which has been associated with abnormal stress responses.²⁷ Thus, there is a potential interrelation between mTBI, cardiac stress responses, and myocardial oxygen delivery. In summary, our study extends the understanding of the cardiac effects of TBI where subclinical diastolic dysfunction and stress-induced dysfunction are seen months after a mild injury

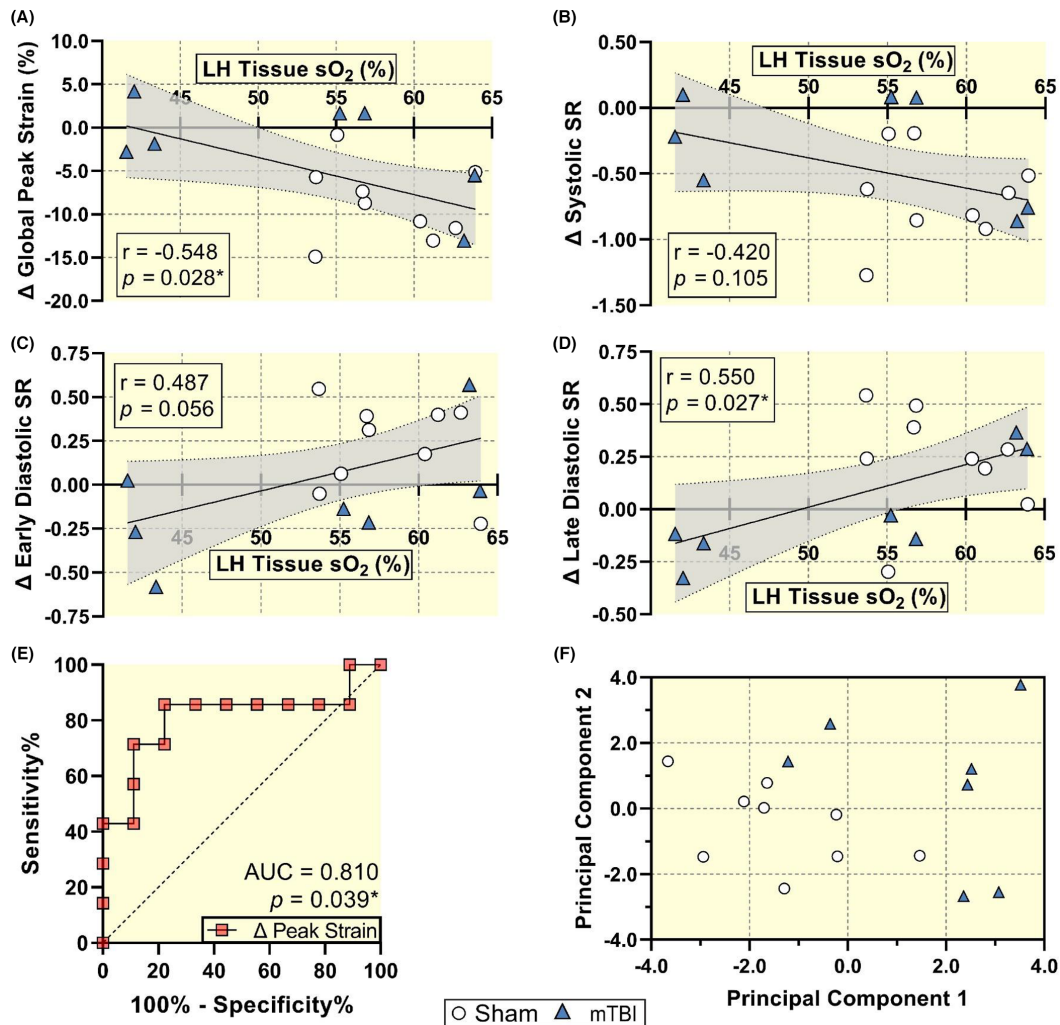


FIGURE 6 Dobutamine stress test cardiac strains correlated with sO₂ 4 h post-injury. Pearson correlation between the dobutamine stress test change in (A) peak strain, (B) systolic strain rate, (C) early diastolic strain rate, (D) late diastolic strain rate and cerebral left hemisphere tissular sO₂ ($n = 16$). All correlation coefficients and the corresponding p -values displayed. (E) ROC analysis of change in peak strain (AUC = 0.810, $p = 0.039$). (F) Principal component analysis results.

using state-of-the-art noninvasive techniques, including PAI and 4DUS, as well as Western blots. How diastolic dysfunction with preserved ejection fraction may relate to long-term clinical management of young mTBI patients warrants further investigation.

3.2 | Molecular imaging and myocardial functional biomarkers after mTBI

Diagnostic tools used post-TBI include computed tomography and magnetic resonance imaging. However, most mTBI show no imaging markers.²⁸ For this reason, patients frequently receive inadequate treatment, particularly children.^{29,30} Our results indicate that PAI and US imaging can be used to evaluate both neurovascular and cardiovascular effects of mTBI, generating noninvasive imaging biomarkers that can be followed longitudinally.

Cerebral PAI shows that the left hemisphere blood oxygenation in the mTBI group was significantly decreased with correlations to sudden behavioral changes. These results align with Ichkova et al.'s work, in which immediate cerebrovascular hypoxia post-TBI was observed.¹¹ Total hemoglobin in the mTBI group was higher than the sham group after 4 h, although this may be influenced by petechial bleeding at the injury site.^{31–33} Furthermore, ROC analyses of acute and long-term neurovascular and cardiac parameters including cerebral sO₂, HbT, and cardiac strain may offer utility in discriminating between the two groups.

Here, a principal component analysis was executed to reduce the dimensionality of multivariate datasets and identify underlying patterns.³⁴ Our results show that combining 13 physiologic measurements from the initial injury and the dobutamine stress test successfully differentiates between sham and mTBI. Hemoglobin was

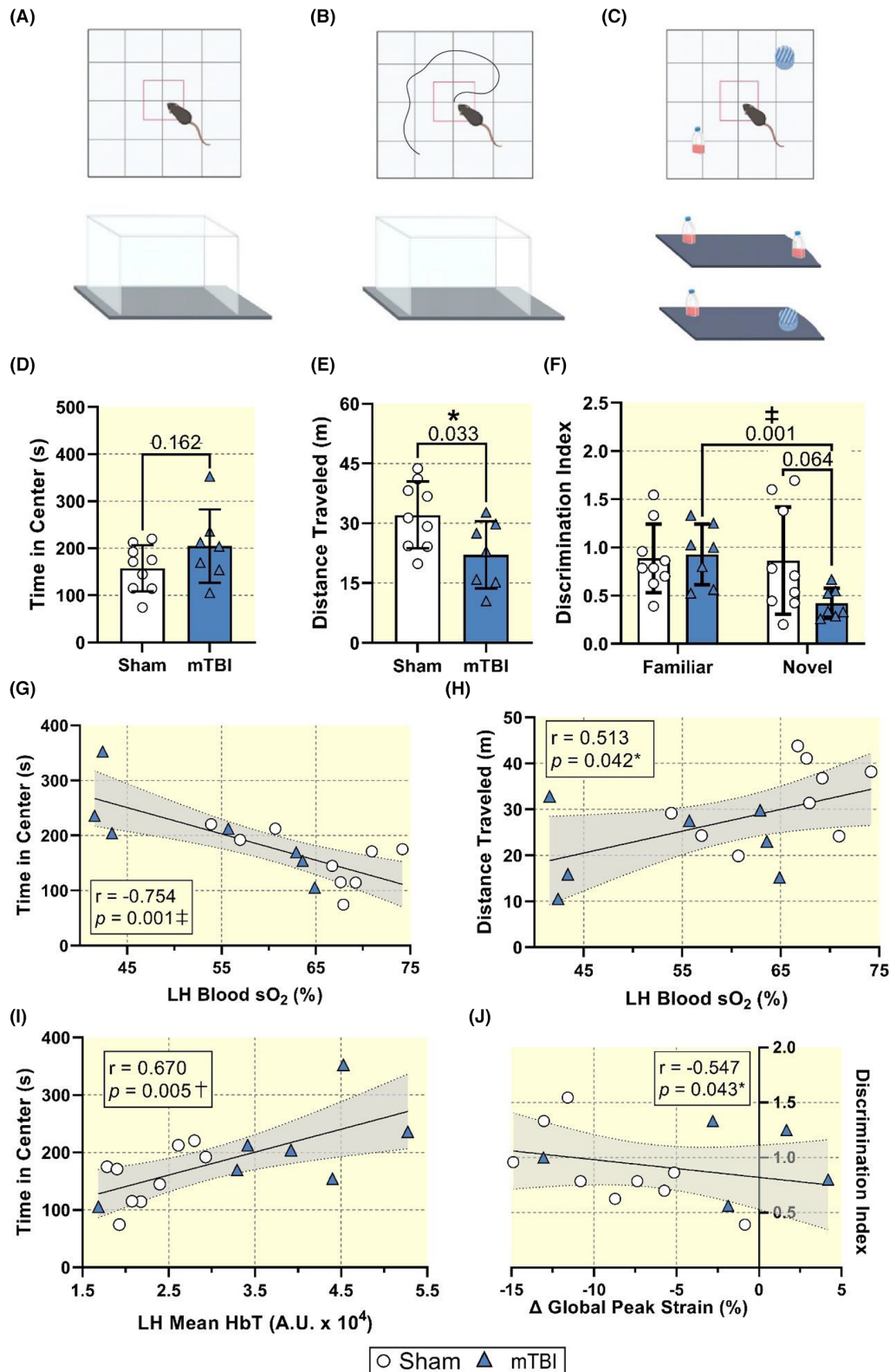


FIGURE 7 Behavior changes in mTBI correlated with initial injury and cardiac outcomes. Experimental design of (A) time in center, (B) distance traveled, and (C) discrimination index behavioral tests. (D) Time in center, (E) distance traveled, and (F) familiar and novel discrimination indices comparisons. (G) Time in center, and (H) distance traveled correlated with left hemisphere blood sO_2 4 h post-injury. Correlation between (I) time in center with left hemisphere mean HbT 4 h post-injury. Correlation between (J) discrimination index and change in global peak strain from the dobutamine stress test. All Pearson correlation coefficients and the corresponding p -values displayed. Sample sizes are sham $n = 9$, mTBI $n = 7$. We used a studentized t -test in subpanels D–E and a two-way ANOVA with Bonferroni post hoc multiple comparisons test in subpanel F.

an important contributor to the differentiation between groups; however, measures of cardiac dysfunction had a larger influence on the analysis than oxygen saturation. These results align with previous work where PCA has been used to discriminate between clinically stratified groups and identify treatment approach factors.^{35,36} Thus, PCA can distinguish between groups and identify underlying variables that may be important in the clinical management of patients with TBI.

3.3 | Neurologic outcomes and long-term cardiac dysfunction associate with initial injury

The long-term effects of mild TBI on the brain and cognitive function have been widely investigated in preclinical and clinical studies.³⁷ Cognitive deficits can appear months or years after the initial injury.³⁸ The long-term effects of mTBI on the brain and cognitive function have been described using our study's model.^{39,40} In agreement with previous works, we show that distance traveled ($p = 0.033$) and discrimination index ($p = 0.064$) were decreased in the mTBI group, which measures locomotor activity and memory recognition, respectively. These results demonstrate the long-term consequences of the mTBI model. We show that long-term neurologic measures correlate with cerebrovascular hypoxia and hemorrhage assessed 4 h after initial mTBI. Thus, acute phase physiologic measurements may offer predictive insights into chronic adulthood and cognitive outcomes that can be used to inform both initial and long-term treatment and biomarkers. A correlation between long-term memory deficits and cardiac dysfunction ($r = -0.547$, $p = 0.043$) shows new potential bidirectional interactions within the heart–brain axis.

The results of this study offer valuable insight into potential clinical and therapeutic interventions. For example, using PAI in mTBI pediatric patients could allow physicians to evaluate neurovascular sO_2 noninvasively immediately post-injury and determine preventive measures to avoid complications. In the acute phase, assessing cardiac TnI levels in the blood could represent a complementary strategy, as increased cardiac TnI is associated with mild and transient impairment of left ventricular function.⁴¹ Pharmacological agents such as beta-blockers have been shown to have cardioprotective effects. They are used in patients suffering from moderate to severe TBI.⁴² Ultrasound, specifically echocardiography, could be used as a noninvasive tool post-TBI to evaluate long-term effects such as left ventricular strain in both relaxed and stressed physiological states.

3.4 | Limitations

The biomechanics underlying human TBI (civilians, sport, or warfare) are heterogeneous as compared to pre-clinical models. However, our methods without a head restraint may replicate some aspects of the unpredictability of TBI in humans. We reported variability in sO_2 levels immediately post-mTBI, suggesting that not all animals experienced a similar mechanism of injury. In our study, this represents an advantage and a variable we fully controlled and stratified using PAI. We also included a representative population of male and female mice, as clinical studies suggest susceptibility for young female athletes experience TBI.^{43,44} We also note that the battery of behavioral testing was fairly limited, but the included tests are standard in rodent studies.³⁹ Finally, our study does not provide long-term structural changes or transcriptional clues to decipher heart–brain modifications occurring post-mTBI; this matter will be investigated as a progression of our research program.

4 | CONCLUSION

In summary, we show that the pathophysiological imprints of mTBI extend beyond the brain to encompass heart functions, with direct correlations unfolding in a time and animal-specific fashion, from juvenile stages to adulthood. Early neurovascular hypoxia seen after mTBI induction could represent a predictive biomarker to assess the risk for long-term maladaptations of the heart–brain axis. These findings support the use of noninvasive modalities to identify and track systemic impacts of mTBI and heart–brain interactions, providing potential avenues to improve patient outcomes.

5 | MATERIALS AND METHODS

5.1 | Animal model

We conducted experiments according to European Directive (2010/63/EU) and the French laws governing laboratory animal use. Local Ethics Committees approved the investigation (authorizations #30489-2021031816059372v2 and #19296-201902191637994v4), and we followed ARRIVE guidelines for animal reporting.⁴⁵ We obtained Swiss breeder mice through Janvier Labs (Le Genest-Saint-Isle, France) and bred mouse pups in-house. The animal environment remained a consistent $21^\circ\text{C} \pm 1^\circ\text{C}$, with $55\% \pm 1\%$ humidity. Animals had access to food and water at all times. Twenty-four mice ($n = 11$ females; $n = 13$ males),

weighing greater than 6 g by post-natal day 17 (P17), were randomly assigned to either a sham ($n = 12$) or mTBI ($n = 12$) experimental group. At P17, the mTBI group underwent a closed head injury procedure, as previously described.¹¹ Photoacoustic brain imaging was acquired 4 h post-injury, and as 7, 30, 90, and 240 days post-injury (Figure 1A,B). Corresponding assessments of cardiac function were made at 1, 30, 90, and 190 days post-injury using two-dimensional ultrasound. Additionally, 4DUS data were acquired at days 7, 30, 90, and 190 post-injury to assess spatially specific cardiac function (Figure 1B). During the dobutamine stress test on day 240 post-injury, both 4DUS and photoacoustic imaging was performed to assess cardiac function and oxygenation, respectively. One-year post-injury, a behavioral evaluation was performed as described below. Of note, one mouse in each group deceased before day 30 and was excluded from the analysis. During the dobutamine stress test, dosing and experimental optimization, reduced sample sizes to sham $n = 9$ and mTBI $n = 7$ for the remaining time points. Analysis of data was blinded to avoid bias.

5.2 | Juvenile mTBI model

We employed a modified closed-head juvenile mTBI model from that previously described.³⁹ Briefly, we anesthetized P17 mice pups with 2.5%–3% isoflurane at 1.5 L/min air for 5 min and subsequently placed them on an aluminum foil sheet under a controlled cortical impactor without a head restraint (Figure 1B). The lack of head restraint allowed for the head rotation observed in concussions, limiting the accumulation of focal damage. Before injury induction, depilatory cream was applied to the cranial area. We performed the mTBI with a controlled cortical impactor (Leica Impact One Stereotaxic impactor, Leica Biosystems, Richmond, IL) with a 3 mm round impactor tip covered with rubber. The impact velocity was 6 m/s with a depth of 3 mm into the head. The tip impacted the left somatosensory parietal cortex 1.7 mm from the bregma and 1.5 mm from the midline. All steps excluding impact were replicated for mice in the sham group. Afterwards, all mice were placed in an empty cage for recovery, the time to ambulate post-anesthesia was recorded.

5.3 | Photoacoustic imaging

PAI was performed with a LAZR-X (Nd:YAG 680–2000 nm) concurrently with the Vevo 3100 (FUJIFILM VisualSonics Inc.) using a 15–30 MHz MX250D probe to

assess brain tissue oxygenation. A depilatory cream was applied on the cranium surface and mice were anesthetized in the supine position with 2.5%–3% isoflurane at 2.0 L/min for the duration of imaging. In preparation for imaging, a heating pad was used to maintain body temperature at 37°C, and ultrasound gel was centrifuged to eliminate bubble artifacts. 3D PAI scan was realized using 80 μ m stacks from the occipital to the frontal brain at 750 and 850 nm (Oxy/De-oxy hemoglobin) excitation wavelengths combined with ultrasound imaging in B-mode. We adjusted the parameters to a PA gain of 40 dB, a 2D gain of 18 dB, an image depth of 22 mm, and an image width of 21 mm. Image acquisition required 4–5 min to obtain approximately 150 frames of PAI data. Neurovascular blood and tissue oxygenation (sO_2) levels (respectively, mean and total oxygen saturation) and mean hemoglobin (HbT) were analyzed offline using VevoLAB (v5.5.1, FUJIFILM VisualSonics).¹⁴

5.4 | Ultrasound imaging

High-resolution 2D and 4DUS data were obtained using the Vevo 3100 high-frequency ultrasound system (FUJIFILM VisualSonics) with a 40-MHz center frequency MX550D probe to assess left ventricular function. Mice were anesthetized with 2.5%–3% isoflurane at 2.0 ml/min, and the body temperature was controlled with a heating pad. We secured the mice to a stage for imaging, and the ventral thorax hair was removed. The ECG and respiratory rate were monitored throughout the imaging process.

We performed 2D echocardiography following the American Physiological Society guidelines for cardiac measurements in mice.⁴⁶ The longitudinal strain was analyzed in the parasternal long-axis (PLAX) view. We obtained a four-chamber view in B-mode to evaluate diastolic dysfunction using IVRT and SrE (2D strain rate at early diastole) in conjunction with LA volume based on 4D data.²⁰ All three measurements give insights into the filling and relaxation of the heart. Offline image analysis was conducted in Vevo Lab Software 5.5.1. (FUJIFILM VisualSonics).

For 4DUS, the probe was attached to a linear step motor scanning in the parasternal short-axis (PSAX) view from below the apex to above the aortic arch. Acquisition parameters were set to a gain of 48 dB, 3D range of 12 mm, 3D step size of 0.08 mm, and frame rate of 300 frames/sec. Each image acquisition required 10–15 min to create 4D data throughout one representative cardiac cycle from base to apex. We analyzed the 4D datasets in a custom, interactive toolbox in MATLAB 2021a (MathWorks, Inc.).

5.5 | Dobutamine stress test

To assess cardiac function under stressed conditions, each mouse had a dose of dobutamine (4.5 $\mu\text{g/g}$ body weight) injected intraperitoneally at day 250 post-impact. 4DUS and PAI data were acquired immediately before dobutamine administration (intraperitoneal injection, 4.5 $\mu\text{g/g}$ body weight) on each animal and 15 min after, which has been indicated to be the plateau phase of the induced stress response.⁴⁷ PAI acquisition was combined with ECG-gated kilohertz visualization (EKV). We adjusted imaging parameters to PA gain of 40 dB, 2D gain of 18 dB, image depth of 22 mm, image width of 21 mm, high PAI sensitivity, and standard acquisition with EKV 250 Hz.

5.6 | Four-dimensional ultrasound data strain analysis

We conducted the strain analysis using a 4D Strain Toolbox. This custom software enables the visualization and quantification of 4DUS data to produce a 3D strain map over an entire cardiac cycle.^{48,49} We first oriented the 4D images and centered them to PLAX, SAX, and coronal views of the left ventricle. Endocardial boundaries were set at peak systole and diastole for the apex and base. Then, we added automated endo- and epicardial contours to the images based on initial estimates. We manually adjusted the contours over the cardiac cycle using four SAX planes and three PLAX planes. Next, the software created a 4D mesh of the contours from which measurements of global cardiac function (e.g., ejection fraction, stroke volume) and regional function (strain, volume) can be extracted.^{48,49} Custom toolbox cardiac wall motion with border tracings can be visualized in Video S1. The cardiac regions included the anterior free wall, anterior septum, posterior septum, posterior, and posterior free wall. The peak strain, systolic strain rate, early diastolic strain rate, and late diastolic strain rate were calculated for each region and then averaged into global strain metrics.

5.7 | Behavioral evaluation

All behavioral tests were conducted at the beginning of the light phase of the cycle. Before testing, the experimenter manipulated the animals for at least a week, which remained blind to the groups throughout the behavioral evaluation. A behavioral assessment was performed over 2 weeks, 1 year after the head trauma. Open field and novel object recognition tests were performed in a custom-made arena with a uniform, smooth black floor (45 \times 45 cm) and gray walls (30 cm tall). The procedure spanned five

consecutive days, and all sessions were recorded and analyzed using Any-Maze (version 7.3, Stoelting Europe). On the first day, animals were habituated to the empty open field for 10 min and constituted the “open field” test with a neutral area. Analyzed parameters were distance traveled, time spent in the center (limited to the center area at least 10 cm away from each wall), and the number of entries into the center area. On days 2–5, novel objection recognition tests lasted 5 min. On days 2–4, two identical objects were positioned in opposite corners, 15 cm away from two consecutive walls. These objects were standard 50 ml transparent culture flasks (4 cm wide, 11 cm tall, and 2.5 cm wide) with a blue cap filled with red-stained sand. The animal is exposed to two identical objects that are, at this point novel, on day 2. Nonetheless, at this timepoint, it is not possible to discriminate non-spatial object memory from pure spatial memory or novelty stimulation. The exposition of the object is repeated twice, on days 3 and 4, such that these objects (as well as the arena) become familiar. On day 5, one of the objects was changed to a novel object consisting of two large white building blocks (8 cm wide, 2 cm tall, and 2.5 cm width) with a smaller light blue building block (6 cm wide, 2 cm tall and 2.5 cm width) in between. The object used on days 2–4 is considered familiar while the object introduced on day 5 is considered novel. An area of 5 cm around each object was defined as the area of interest. The number of entries represented the number of interactions with the object, and the time spent in the area represented the time spent interacting with the object. This allows us to evaluate the capacity of the animal to form nonspatial object memory through the discrimination index.

5.8 | Western blot analysis

To assess early cardiac biochemistry changes, we used a Simple Western™ Automated Western Blot Systems as previously described⁵⁰ to detect total p38 MAPK and cardiac TnI expression level in both sham ($n = 6$) and mTBI ($n = 6$) mice 30 days after mTBI. Based on capillary electrophoresis, a Simple Western is a reinvention of the Western blot technique allowing for the complete automation of steps from protein loading to quantitative data analysis.⁵¹ Briefly, 1-month post-mTBI, animals were euthanized. Cardiac tissue samples were collected and prepared for Western blot. Cardiac protein lysate was mixed with a fluorescent mix before heating at 95°C for 5 min. Total protein normalization agent, blocking reagent, 3 μl of protein mix, wash buffer, primary antibody, secondary HRP (ready to use “detection module,” DM-001), and a chemiluminescent substrate were added into designated wells in a microplate. We used T-p38 MAPK antibody

(cst#9218; Cell Signaling Technology) and TnI (cst#4002; Cell Signaling Technology). Once loaded into the instrument, the protein mix was drawn into individual capillaries on a manufacturer 25 capillary cassette (12–230 kDa or 66–440 kDa). Quantification of chemiluminescence was based on peak height after correction for a baseline signal. Raw data were generated and analyzed by Compass software.

5.9 | Statistical analysis

We conducted a two-way ANOVA with a Bonferroni post hoc multiple comparisons test to investigate differences between groups at multiple time points. For comparisons between groups without repeat measurement comparisons, we checked for normality with a Shapiro–Wilk test. Normally distributed data were compared with two-tailed unpaired Student's *t*-tests. We set the threshold for statistical significance at $p < 0.05$, and levels of significance were depicted as $p < 0.05^*$, $p < 0.01^\dagger$, and $p < 0.001^\ddagger$. Correlation between quantified metrics was described using Pearson correlation coefficients if a Shapiro–Wilk test indicated data normality; otherwise, a Spearman's correlation coefficient was calculated. Only animals with data for all metrics of interest were included in the correlation analyses. All data are shown as mean \pm standard deviation (SD). All statistical analysis was performed using Prism 9.3 (GraphPad Software). The correlation coefficients, *r*, and corresponding *p*-values are displayed.

A receiver operating characteristic (ROC) analysis was performed to evaluate acute photoacoustic and long-term echocardiographic biomarkers to discriminate between sham and mTBI animals. Acute photoacoustic biomarkers include left hemisphere blood sO_2 , tissue sO_2 , and mean HbT in sham ($n = 11$) and mTBI ($n = 11$) mice 4 h post-TBI. Long-term echocardiography markers include the changes in strain and strain rates from the dobutamine stress test 250 days post-mTBI. A 95% confidence interval with a hybrid Wilson/Brown method were employed during this analysis and the area under the curve (AUC) was computed to determine the model's ability to distinguish between the groups at various thresholds.

Principal component analysis (PCA) was run to determine new meaningful underlying variables, and included all dobutamine stress test 4DUS derived strain metrics, cardiac perfusion, left hemisphere brain oxygenation, and hemoglobin at 4 h post-injury. The analysis did not include behavioral outcomes. We used a standardized PCA method due to the different measurement scales of the variables included. Principal components (PCs) were

selected based on parallel analysis with 1000 simulations and a 95% percentile level. We plotted the first two PCs against one another to distinguish between the two groups. The contributions of a variable to PC1 and PC2 were averaged to evaluate the overall importance. All material submitted conforms to good publishing practice in physiology.⁵²

AUTHOR CONTRIBUTIONS

KL, JPS designed, planned, and performed the 4D strain analysis and most of the experimental work including data analysis; prepared the figures; and drafted the manuscript. NP initiated, planned, and led the study; performed the mTBI model in mice and US/PA imaging in the heart and brain; analyzed 2D and PA images; and drafted the manuscript. FD helped in the initial stages of the project with 4D data analysis. AJ, EZ provided technical training and helped with the preparation for in vivo studies. CB performed and analyzed the Western blot data. RR, CJD performed and analyzed behavior data included in Figure 7. JB, provided training and advice on the mTBI model throughout the project. SR provided advice on the project, reviewed, and edited the manuscript. NM, CJG, and PS initiated, designed, and provided continuous guidance in the conceptual design of the work, data interpretation, reviewed and edited the manuscript. All the authors edited and approved the manuscript.

ACKNOWLEDGMENTS

We gratefully thank the staff for animal housing (PhyMedExp) and Imagerie du Petit Animal de Montpellier (IPAM) for accessing high-resolution ultrasound and photoacoustic imaging. (LRQA Iso9001; France Life Imaging (grant ANR-11-INBS-0006); IBISA; Leducq Foundation (RETP), I-Site Muse). We acknowledge the technical support provided by the We-Met Biochemistry platform (I2MC, Toulouse; info@we-met.fr).

FUNDING INFORMATION

Fulbright United States Scholar Program (CG), Chateaubriand Fellowship (KL), Montpellier Advanced Knowledge Institute on Transitions Program of the Université de Montpellier (CG), Thomas Jefferson Fund from the French-American Cultural Exchange Foundation (CG, PS), Biocampus (PS), I-Site Muse (PS), Era-Net ANR 2019 NeuVasc (NM and JB), and ANR Epicatcher (NM).

CONFLICT OF INTEREST

All authors have read the journal's policy on disclosure of potential conflicts of interest. C. J. Goergen serves on the Scientific Advisory Board for FUJIFILM VisualSonics

Inc. None of the other authors have conflicts of interest, financial or otherwise, to disclose. Disclaimers: FUJIFILM VisualSonics Inc. had no role in the study's design, execution, interpretation, or writing.

DATA AVAILABILITY STATEMENT

Data will be made available upon reasonable request.

ORCID

Katherine Leyba  <https://orcid.org/0000-0003-3548-3391>

Pierre Sicard  <https://orcid.org/0000-0001-5837-3916>

REFERENCES

- Dewan MC, Rattani A, Gupta S, et al. Estimating the global incidence of traumatic brain injury. *J Neurosurg*. 2018;130(4):1080-1097. doi:10.3171/2017.10.JNS17352
- Ouellet MC, Beaulieu-Bonneau S, Morin CM. Traumatic brain injury. *Handb Sleep Disord Med Cond*. 2022;1(1):221-252. doi:10.1016/B978-0-12-813014-8.00010-X
- van Vliet EA, Marchi N. Neurovascular unit dysfunction as a mechanism of seizures and epilepsy during aging. *Epilepsia*. 2022;63(6):1297-1313. doi:10.1111/EPI.17210
- McDonald SJ, Sharkey JM, Sun M, et al. Beyond the brain: peripheral interactions after traumatic brain injury. *J Neurotrauma*. 2020;37(5):770-781. doi:10.1089/neu.2019.6885
- Hasanin A, Kamal A, Amin S, et al. Incidence and outcome of cardiac injury in patients with severe head trauma. *Scand J Trauma Resusc Emerg Med*. 2016;24:58. doi:10.1186/s13049-016-0246-z
- Izzy S, Chen PM, Tahir Z, et al. Association of traumatic brain injury with the risk of developing chronic cardiovascular, endocrine, neurological, and psychiatric disorders. *JAMA Netw Open*. 2022;5(4):e229478. doi:10.1001/jamanetworkopen.2022.9478
- Delage C, Taib T, Mamma C, Lerouet D, Besson VC. Traumatic brain injury: an age-dependent view of post-traumatic neuroinflammation and its treatment. *Pharmaceutics*. 2021;13(10):1624. doi:10.3390/pharmaceutics13101624
- Owens TS, Calverley TA, Stacey BS, et al. Concussion history in rugby union players is associated with depressed cerebrovascular reactivity and cognition. *Scand J Med Sci Sports*. 2021;31(12):2291-2299. doi:10.1111/SMS.14046
- Lumba-Brown A, Yeates KO, Sarmiento K, et al. Diagnosis and management of mild traumatic brain injury in children: a systematic review. *JAMA Pediatr*. 2018;172(11):e182847. doi:10.1001/jamapediatrics.2018.2847
- Krishnamoorthy V, Prathep S, Sharma D, Fujita Y, Armstead W, Vavilala MS. Cardiac dysfunction following brain death after severe pediatric traumatic brain injury: a preliminary study of 32 children. *Int J Crit Illn Inj Sci*. 2015;5(2):103-107. doi:10.4103/2229-5151.158409
- Ichkova A, Rodriguez-Grande B, Zub E, et al. Early cerebrovascular and long-term neurological modifications ensue following juvenile mild traumatic brain injury in male mice. *Neurobiol Dis*. 2020;141:104952. doi:10.1016/j.nbd.2020.104952
- Xia J, Yao J, Wang LV. Photoacoustic tomography: principles and advances. *Electromagn Waves*. 2014;147:1-22. doi:10.2528/pier14032303
- Saeed M, Anh Van T, Krug R, Hetts SW, Wilson MW. Cardiac MR imaging: current status and future direction. *Cardiovasc Diagn Ther*. 2014;5(4):290-310. doi:10.3978/j.issn.2223-3652.2015.06.07
- David H, Ughetto A, Gaudard P, et al. Experimental myocardial infarction elicits time-dependent patterns of vascular hypoxia in peripheral organs and in the brain. *Front Cardiovasc Med*. 2021;7:615507. doi:10.3389/fcvm.2020.615507
- Sicard P, Jouitteau T, Andrade-Martins T, et al. Right coronary artery ligation in mice: a novel method to investigate right ventricular dysfunction and biventricular interaction. *Am J Physiol Hear Circ Physiol*. 2019;316(3):H684-H692. doi:10.1152/ajpheart.00573.2018
- Damen FW, Berman AG, Soepriatna AH, et al. High-frequency 4-dimensional ultrasound (4DUS): a reliable method for assessing murine cardiac function. *Tomography*. 2017;3(4):180-187. doi:10.18383/j.tom.2017.00016
- Zipes DP, Libby P, Bonow RO, Mann DL, Tomaselli GF, Braunwald E. *Braunwald's Heart Disease: A Textbook of Cardiovascular Medicine*. Vol. 2. 11th ed. Elsevier; 2018.
- Bailes JE, Dashnaw ML, Petraglia AL, Turner RC. Cumulative effects of repetitive mild traumatic brain injury. *Prog Neurol Surg*. 2014;28:50-61. doi:10.1159/000358765
- Gregory MTS. Cardiovascular complications of brain injury. In: Langton JA, ed. *Continuing Education in Anesthesia, Critical Care, and Pain* (Vol. 12, 2nd ed.). Oxford University Press; 2011:67-71. doi:10.1093/bjaceaccp/mkr058
- Schnelle M, Catibog N, Zhang M, et al. Echocardiographic evaluation of diastolic function in mouse models of heart disease. *J Mol Cell Cardiol*. 2018;114:20-28. doi:10.1016/j.yjmcc.2017.10.006
- Cuisinier A, Maufrais C, Payen JF, Nottin S, Walther G, Bouzat P. Myocardial function at the early phase of traumatic brain injury: a prospective controlled study. *Scand J Trauma Resusc Emerg Med*. 2016;24(1). doi:10.1186/S13049-016-0323-3
- Murphy AM, Kogler H, Georgakopoulos D, et al. Transgenic mouse model of stunned myocardium. *Science*. 2000;287(5452):488-491. doi:10.1126/science.287.5452.488
- Tenhunen O, Rysa J, Ilves M, Soini Y, Ruskoaho H, Leskinen H. Identification of cell cycle regulatory and inflammatory genes as predominant targets of p38 mitogen-activated protein kinase in the heart. *Circ Res*. 2006;99(5):485-493. doi:10.1161/01.RES.0000238387.85144.92
- Krishnamoorthy V, Chaikittisilpa N, Lee J, et al. Speckle tracking analysis of left ventricular systolic function following traumatic brain injury: a pilot prospective observational cohort study. *J Neurosurg Anesthesiol*. 2020;32(2):156-161. doi:10.1097/ANA.0000000000000578
- Sturgill MG, Kelly M, Notterman DA. Pharmacology of the cardiovascular system. *Pediatr Crit Care*. 2011;29:277-305. doi:10.1016/B978-0-323-07307-3.10025-4
- Abouezzeddine OF, Kemp BJ, Borlaug BA, et al. Myocardial energetics in heart failure with preserved ejection fraction. *Circ Hear Fail*. 2019;12(10):e006240. doi:10.1161/CIRCHEARTFAILURE.119.006240
- van Empel VP, Mariani J, Borlaug BA, Kaye DM. Impaired myocardial oxygen availability contributes to abnormal exercise hemodynamics in heart failure with preserved ejection fraction. *J Am Hear Assoc*. 2014;3(6):e001293. doi:10.1161/JAHA.114.001293

28. Bigler ED, Abildskov TJ, Goodrich-Hunsaker NJ, et al. Structural neuroimaging findings in mild traumatic brain injury. *Sports Med Arthrosc.* 2016;24(3):e42. doi:[10.1097/JSA.0000000000000119](https://doi.org/10.1097/JSA.0000000000000119)
29. Bigler ED. Systems biology, neuroimaging, neuropsychology, neuroconnectivity and traumatic brain injury. *Front Syst Neurosci.* 2016;10:55. doi:[10.3389/fnsys.2016.00055](https://doi.org/10.3389/fnsys.2016.00055)
30. Amyot F, Arciniegas DB, Brazaitis MP, et al. A review of the effectiveness of neuroimaging modalities for the detection of traumatic brain injury. *J Neurotrauma.* 2015;32(22):1693-1721. doi:[10.1089/neu.2013.3306](https://doi.org/10.1089/neu.2013.3306)
31. Kurland D, Hong C, Aarabi B, Gerzanich V, Simard JM. Hemorrhagic progression of a contusion after traumatic brain injury: a review. *J Neurotrauma.* 2012;29(1):19-31. doi:[10.1089/neu.2011.2122](https://doi.org/10.1089/neu.2011.2122)
32. Demené C, Robin J, Dizeux A, et al. Transcranial ultrafast ultrasound localization microscopy of brain vasculature in patients. *Nat Biomed Eng.* 2021;5(3):219-228. doi:[10.1038/s41551-021-00697-x](https://doi.org/10.1038/s41551-021-00697-x)
33. Barud M, Dabrowski W, Siwicka-Gieroba D, Robba C, Bielacz M, Badenes R. Usefulness of cerebral oximetry in TBI by NIRS. *J Clin Med.* 2021;10(13). doi:[10.3390/jcm10132938](https://doi.org/10.3390/jcm10132938)
34. Jolliffe IT, Cadima J. Principal component analysis: a review and recent developments. *Philos Trans R Soc A Math Phys Eng Sci.* 2016;374(2065):20150202. doi:[10.1098/RSTA.2015.0202](https://doi.org/10.1098/RSTA.2015.0202)
35. Ljubicic ML, Madsen A, Juul A, Almstrup K, Johannsen TH. The application of principal component analysis on clinical and biochemical parameters exemplified in children with congenital adrenal hyperplasia. *Front Endocrinol (Lausanne).* 2021;12:1057. doi:[10.3389/FENDO.2021.652888/BIBTEX](https://doi.org/10.3389/FENDO.2021.652888/BIBTEX)
36. Andkhoie M, Meyer D, Szafron M. Factors underlying treatment decision-making for localized prostate cancer in the U.S. and Canada: a scoping review using principal component analysis. *Can Urol Assoc J.* 2019;13(7):E220. doi:[10.5489/CUAJ.5538](https://doi.org/10.5489/CUAJ.5538)
37. Danna-Dos-Santos A, Mohapatra S, Santos M, Degani AM. Long-term effects of mild traumatic brain injuries to oculomotor tracking performances and reaction times to simple environmental stimuli. *Sci Rep.* 2018;8(1):4583. doi:[10.1038/s41598-018-22825-5](https://doi.org/10.1038/s41598-018-22825-5)
38. Dean PJ, Sterr A. Long-term effects of mild traumatic brain injury on cognitive performance. *Front Hum Neurosci.* 2013;7:30. doi:[10.3389/fnhum.2013.00030](https://doi.org/10.3389/fnhum.2013.00030)
39. Rodriguez-Grande B, Obenaus A, Ichkova A, et al. Gliovascular changes precede white matter damage and long-term disorders in juvenile mild closed head injury. *Glia.* 2018;66(8):1663-1677. doi:[10.1002/glia.23336](https://doi.org/10.1002/glia.23336)
40. Clément T, Lee JB, Ichkova A, et al. Juvenile mild traumatic brain injury elicits distinct spatiotemporal astrocyte responses. *Glia.* 2020;68(3):528-542.
41. El-Menyar A, Sathian B, Wahlen BM, Al-Thani H. Serum cardiac troponins as prognostic markers in patients with traumatic and non-traumatic brain injuries: a meta-analysis. *Am J Emerg Med.* 2019;37(1):133-142. doi:[10.1016/j.ajem.2018.10.002](https://doi.org/10.1016/j.ajem.2018.10.002)
42. Nguemu S, Meloni M, Endalle G, et al. Paroxysmal sympathetic hyperactivity in moderate-to-severe traumatic brain injury and the role of Beta-blockers: a scoping review. *Emerg Med Int.* 2021;2021:5589239. doi:[10.1155/2021/5589239](https://doi.org/10.1155/2021/5589239)
43. Bretzin AC, Covassin T, Fox ME, et al. Sex differences in the clinical incidence of concussions, missed school days, and time loss in high school student-athletes: part 1. *Am J Sports Med.* 2018;46(9):2263-2269. doi:[10.1177/0363546518778251](https://doi.org/10.1177/0363546518778251)
44. Zhang YP, Cai J, Shields LBE, Liu N, Xu XM, Shields CB. Traumatic brain injury using mouse models. *Transl Stroke Res.* 2014;5(4):454-471. doi:[10.1007/S12975-014-0327-0](https://doi.org/10.1007/S12975-014-0327-0)
45. du Sert NP, Ahluwalia A, Alam S, et al. Reporting animal research: explanation and elaboration for the arrive guidelines 2.0. *PLoS Biol.* 2020;18(7). doi:[10.1371/JOURNAL.PBIO.3000411](https://doi.org/10.1371/JOURNAL.PBIO.3000411)
46. Lindsey ML, Kassiri Z, Virag JAI, de Castro Bras LE, Scherrer-Crosbie M. Guidelines for measuring cardiac physiology in mice. *Am J Physiol Hear Circ Physiol.* 2018;314(4):H733-H752. doi:[10.1152/ajpheart.00339.2017](https://doi.org/10.1152/ajpheart.00339.2017)
47. Salami CO, Jackson K, Jose C, et al. Stress-induced mouse model of the cardiac manifestations of Friedreich's ataxia corrected by AAV-mediated. *Gene Ther.* 2020;31(15-16):819-827. doi:[10.1089/hum.2019.363](https://doi.org/10.1089/hum.2019.363)
48. Damen FW, Salvas JP, Pereyra AS, Ellis JM, Goergen CJ. Improving characterization of hypertrophy-induced murine cardiac dysfunction using four-dimensional ultrasound-derived strain mapping. *Am J Physiol Hear Circ Physiol.* 2021;321(1):H197-H207. doi:[10.1152/ajpheart.00133.2021](https://doi.org/10.1152/ajpheart.00133.2021)
49. Dann MM, Clark SQ, Trzaskalski NA, et al. Quantification of murine myocardial infarct size using 2-D and 4-D high-frequency ultrasound. *Am J Physiol Hear Circ Physiol.* 2022;322(3):H359-H372. doi:[10.1152/ajpheart.00476.2021](https://doi.org/10.1152/ajpheart.00476.2021)
50. Moreira Souza AC, Grabe-Guimarães A, Cruz J d S, et al. Mechanisms of artemether toxicity on single cardiomyocytes and protective effect of nanoencapsulation. *Br J Pharmacol.* 2020;177(19):4448-4463. doi:[10.1111/BPH.15186](https://doi.org/10.1111/BPH.15186)
51. Nguyen U, Squaglia N, Boge A, Fung PA. The simple Western™: a gel-free, blot-free, hands-free Western blotting reinvention. *Nat Methods.* 2011;8(11):v-vi. doi:[10.1038/nmeth.f.353](https://doi.org/10.1038/nmeth.f.353)
52. Jensen BL, Persson PB. Good publication practice in physiology 2021. *Acta Physiol.* 2022;234(1):e13741. doi:[10.1111/APHA.13741](https://doi.org/10.1111/APHA.13741)

SUPPORTING INFORMATION

Additional supporting information can be found online in the Supporting Information section at the end of this article.

How to cite this article: Leyba K, Paiyabhroma N, Salvas JP, et al. Neurovascular hypoxia after mild traumatic brain injury in juvenile mice correlates with heart-brain dysfunctions in adulthood. *Acta Physiol.* 2023;238:e13933. doi:[10.1111/apha.13933](https://doi.org/10.1111/apha.13933)